Journal of Power Sources 226 (2013) 162–172

Contents lists available at SciVerse ScienceDirect

Journal of Power Sources

journal homepage: www.elsevier.com/locate/jpowsour

Ni/YSZ pattern anodes fabrication and their microstructure and electrochemical behavior changes in H_2–H_2O environments

W. Yao, E. Croiset*

Department of Chemical Engineering, University of Waterloo, 200 University Avenue West, Waterloo Ontario, N2L 3G1, Canada

HIGHLIGHTS

- Ni/YSZ pattern anodes were fabricated by a bi-layer lift-off method.
- Ni thickness, temperature, and H_2O content affect Ni pattern microstructure.
- High H_2O content leads to fast degradation of the pattern anode above 700 °C.
- The cell can be pre-treated in H_2 at 750 or 800 °C to accelerate its stabilization.

ARTICLE INFO

Article history:
Received 18 July 2012
Received in revised form
14 October 2012
Accepted 15 October 2012
Available online 26 October 2012

Keywords:
Solid oxide fuel cell
Ni/YSZ pattern anode
Bi-layer lift-off method
Ni pattern microstructure
Ni pattern stability

ABSTRACT

An effective photolithographic process was investigated to fabricate Ni/YSZ pattern anodes using a bi-layer lift-off resist method. Suitable undercut size was found critical for successful pattern fabrication. Effects of Ni thickness, temperature and H_2O content on Ni pattern microstructure were evaluated. Ni/YSZ pattern anodes with 0.5 μm thick Ni was tested in dry H_2 at 550 °C without significantly changing the TPB line. Ni/YSZ pattern anodes with Ni thickness of 0.8 μm were tested at 550 °C under dry and humidified H_2 (3–50% H_2O) conditions without TPB line change. At 700 °C, and for 0.8 μm thick patterns, the TPB length showed pronounced change in H_2 with 10–50% H_2O. Significant increase in TPB length due to holes formation was observed at 800 °C with 3% and 10% H_2O. Ni/YSZ pattern anodes with 1.0 μm thick Ni was stable in H_2 with 3% H_2O in the range 550–800 °C, with TPB line only slightly modified. However, distinct change of TPB line and Ni microstructure was observed with 10–70% H_2O above 700 °C. Stabilization of the polarization resistance depends on temperature. To accelerate stabilization of the cell, pre-treatment of the cell in H_2 with 3% H_2O at 750 °C or 800 °C could be performed.

1. Introduction

Solid oxide fuel cell (SOFC) represents a promising technology that converts chemical energy directly to electrical energy cleanly and efficiently. SOFCs can operate with a wide range of fuels and have significantly lower environmental footprint than combustion systems [1–3]. However, problems such as poor long-term stability and high cost exist in current SOFCs development, hence motivating efforts to improve the SOFC performance and lower the cost. High internal loss contributes to the low cell performance. Furthermore, anodic loss can represent a significant part of the overall loss, in particular in anode supported cells; therefore, it is desirable to reduce the anodic loss in order to enhance the overall cell performance. Understanding the actual elementary reaction steps occurring at the anode is important to further improve the anode performance. However, even for the simplest fuel, H_2, the detailed electrochemical reactions are not yet fully understood [4–7].

The electrochemical reactions take place at the triple phase boundary (TPB), where gas phase, anode and electrolyte meet [5,6,8].

For reaction kinetic studies, pattern anodes have the advantage of forming a well-defined structure, which means that, in principle, the TPB length can be measured accurately.

Yttria-Stabilized Zirconia (YSZ) is currently the state-of-art electrolyte material for SOFC and Ni/YSZ pattern anodes have been widely used in fuel electrochemical reaction mechanism studies [3–12].

Ni/YSZ pattern anodes with a well-defined structure mean that the translation of the pattern from the mask to the substrate is accurate. Besides, the corner and edge of the pattern should be

* Corresponding author. Tel.: +1 519 888 4567x36472/32295; fax: +1 519 746 4979.
E-mail addresses: ecroiset@cape.uwaterloo.ca, ecroiset@uwaterloo.ca (E. Croiset).

0378-7753/$ – see front matter © 2012 Elsevier B.V. All rights reserved.
http://dx.doi.org/10.1016/j.jpowsour.2012.10.053

precise and sharp. Thus, the TPB length can be accurately calculated. Furthermore, precise control of the photolithographic process becomes the critical step in the fabrication of pattern anodes.

There are two traditional methods to make Ni/YSZ pattern anodes: 1) chemical etching and 2) lift-off. Both methods include photolithography and Ni thin film deposition processes.

Chemical etching is a common way to make micro-patterns on a substrate by using chemical etchant. In this process, the metal thin film is first deposited on the substrate surface, and then the photoresist is coated and patterned. After immersing the patterned substrate in the etchant, the metal film region without photoresist covered is etched away, and the region with photoresist covered stays [13]. Details of this process are shown in Fig. 1(a).

Lift-off is another way to make micro-patterns. Different from chemical etching, the photoresist is spun on the clean substrate and patterned. Then, a metal thin film is deposited on the patterned substrate. The metal film with photoresist underneath is washed away by a remover, and the metal film directly deposited on the metal film remains. Therefore, the desired thin film pattern is fabricated [13]. Fig. 1(b) describes the lift-off process.

1.1. Photolithography

Photolithography is a process which transfers patterns defined on a mask to a substrate. The pattern on the mask is first transferred to a photoresist, which experiences chemical structure changes under exposure to a radiation source. Two types of photoresist (positive and negative photoresists) can be used for the photolithographic process [14,15].

Exposing the positive photoresist to ultraviolet light (UV) shone through a mask with the desired pattern changes the chemical structure of the exposed photoresist region. Therefore, it becomes more soluble in the developer solution, and can be easily stripped, leaving the unexposed region behind. Different from the positive photoresist, exposed region of the negative photoresist through the mask becomes polymerized, and is insoluble in the developer solution, thus remaining on the substrate. Meanwhile, the unexposed region is removed by the developer solution [13].

1.2. Metal deposition

Physical vapor deposition (PVD) is a physical process transferring atoms or molecules from source material to the substrate surface and is extensively used for thin film deposition. PVD has the advantage of depositing high quality thin films. Electron-beam evaporation (namely E-beam evaporation) and DC magnetron sputtering are two typical PVD processes [16–18]. These two methods were commonly used to fabricate patterned electrodes in previous Ni pattern studies [3–5,7,9–12,14].

In the E-beam evaporation process, the source material is heated to the boiling and evaporating point by a focused electron beam. The evaporated molecules move freely in the chamber due to the high vacuum ($\sim 10^{-6}$ mbar), and precipitate on all solid surfaces. In addition, high chamber vacuum also minimizes existence of background gas, and increases the mean free path of metal particles. Therefore, the metal film has less chance to be contaminated and sidewalls are not likely to be coated with the metal film [15].

During DC magnetron sputtering, a target with the source material and an arrangement of permanent magnets are used. The magnets generate a magnetic field to capture the electrons. The collision between electrons and inert sputtering gas atoms (Argon) creates Argon ions. By applying negative voltage to the target, Argon ions are accelerated toward the target, and eject atoms from the target material [15,16,18].

Compared to evaporation process, DC sputtering has the advantage of depositing uniform thickness film on the substrate. Besides, the metal film grain size and stress between the film and substrate can be well controlled. Furthermore, the sputtering process allows better adhesion between the deposited film and substrate [14,15].

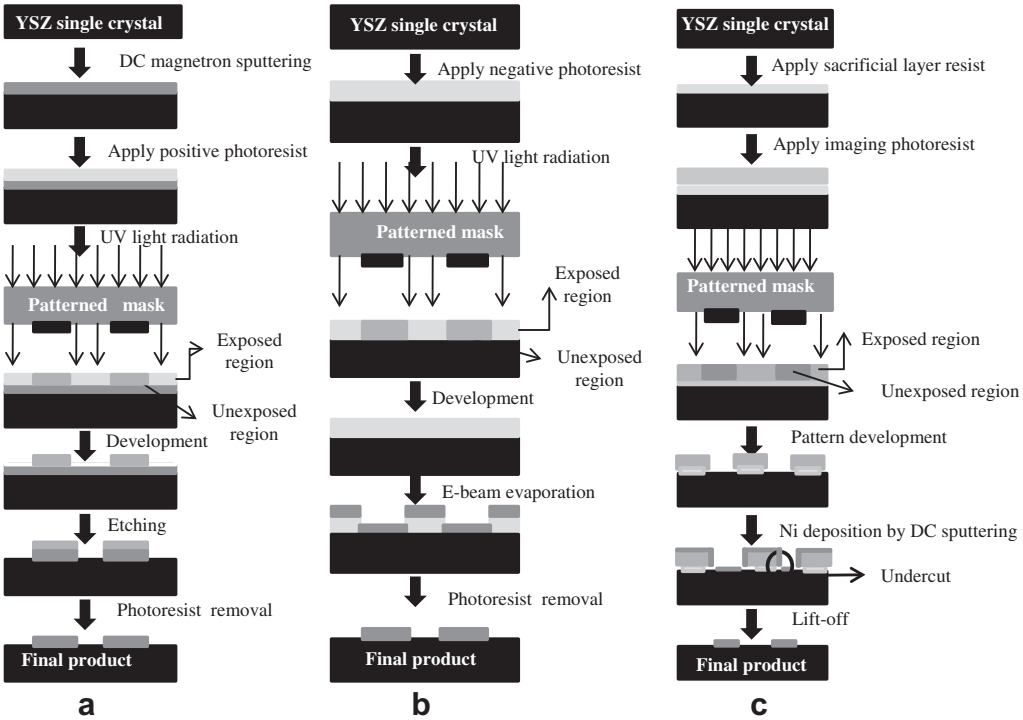

Fig. 1. Microstructure fabrication processes (a) Chemical etching, (b) Lift-off, (c) Bi-layer lift-off.

1.3. Related work

Although several groups fabricated Ni/YSZ pattern anodes for kinetic studies, none of them clearly mentioned fabrication details. Besides, the fabrication technique is extremely sensitive and requires very fine tuning of several fabrication parameters. There are also some parameters that are difficult to control but that must be taken into account, like pre-bake temperature of the resist on a hotplate and the inconsistent shaking during the development process.

Chemical etching has been used in several studies for making Ni/YSZ pattern anode [3–5,8,11,12].

Although chemical etching is easy to perform, it is hard to control, and over-etching always happens. It is extremely difficult to make the anode with smooth and sharp patterns by this method, which further reduces the accuracy of TPB length calculation. Lift-off can also be used for pattern anodes fabrication; however, the evaporation technique used in this process limits the thickness of Ni film deposited on the substrate. Furthermore, adhesion between Ni and YSZ is weak.

More recently, Stormer's group at Karlsruhe University demonstrated a new method for pattern anode fabrication with better defined TPB length [7,9,10]. This method involves using a bi-layer resist system (sacrificial and imaging resists) for photolithography. The sacrificial resist is not photoactive, but can create an undercut, which is critical for effective lift-off after Ni deposition by DC sputtering. The undercut ensures the discontinuity of the side wall films and horizontal films after sputtering, so the resist structure and unwanted Ni films can be removed cleanly by lift-off [7,14]. The process of photolithography with bi-layer resist system is shown in Fig. 1(c).

Based on the same idea of creating undercut, we tried two different imaging resists for pattern anode fabrication. It turned out that the bi-layer resist system is very effective for the Ni/YSZ pattern anode fabrication when proper imaging and sacrificial resists are used.

In the literature, several studies [3–5,7–9,11,12] were conducted to investigate the electrochemical behavior of Ni/YSZ pattern anodes in H_2–H_2O environments. Most of these studies have shown that polarization resistance of the anode decreases when increasing the water partial pressure, temperature, overpotential and hydrogen partial pressure. However, there is no consensus regarding activation energy, charge transfer coefficient, hydrogen reaction order and water reaction order. Moreover, the qualitative value of polarization resistance is shown to be quite different from one research group to another. Differences between these studies maybe due to the impurity level, inaccurate estimation of active TPB length, and even the time at which data were collected [7,11]. Therefore, it becomes extremely important to better understand the microstructure changes of Ni/YSZ pattern anodes before evaluating detailed electrochemical processes.

2. Experiments

2.1. SOFCS with Ni/YSZ pattern anodes fabrication

The electrolyte used in this study is an 8% mol Y_2O_3 stabilized ZrO_2 single crystal disc with (100) orientation (MTI corporation). It is a 0.5" × 0.5" square disc with both sides polished, and both sides having the same roughness (<5 Å by AFM).

YSZ single crystal was chosen to ensure successful photolithography. Positive masks were used in this study, and they were fabricated by a commercial company (Fineline Imaging Laser Imaged Phototooling). Those masks are patterned chrome on soda lime glasses.

The design of Ni/YSZ pattern anode is given by Fig. 2.

The photolithographic process, and in particular the choice of resist, plays an important role for the successful micro-pattern fabrication. In this study, various fabrication conditions were optimized, such as selection of photoresists, exposure time, spin speeds for both sacrificial and imaging resists, soft-bake temperature and development time.

MicroChem's resist polydimethyl glutarimide (PGMI) S11 was used as sacrificial layer. Negative photoresist nLOF2035 (AZ Electronic Materials) or ma-N-1420 (Micro Resist Technology) were used as imaging layer.

Before performing photolithography, YSZ substrates were cleaned by acetone, isopropyl alcohol (IPA), deionized (DI) water and RCA solution (H_2O: NH_3OH: H_2O_2 = 1:5:5) in that order. Then, YSZ substrates were dried up on a hotplate for 10 min at 160 °C.

Sacrificial resist PGMI S11 was spun on the clean YSZ surface at 4500 rpm for 45 s. After that, the substrate was placed on a vacuum hotplate for soft-bake at 160 °C for 5 min. Then, the substrate was cooled down to room temperature, and the imaging photoresist nLOF2035 was spin coated at 3000 rpm for 30 s. Soft-bake conditions for imaging photoresist were 110 °C, for 1 min. After cooling down, the substrate was placed in a mask aligner (Oriel Corp). Meanwhile, the mask was loaded on the mask holder. Both positions of the mask and the YSZ substrate were adjusted to make perfect contact, so that the patterns on the mask were transferred to the YSZ.

Ultraviolet Illumination System (Oriel Corp.) was used for providing UV radiation and the photoresist was exposed for 14 s. Before development, post exposure bake was conducted at 110 °C for 1 min. The photoresist pattern development was performed in an AZ300 MIF (metal ion free) developer solution (AZ Electronic Materials) at room temperature. The development time was optimized in order to create suitable undercut which helps the lift-off process. Then, the substrate with photoresist pattern was deposited with nickel by DC magnetron sputtering.

The size of Ni target in this study was 6" dia. × 0.125", and its purity was 99.99%. The parameters in Table 1 were chosen for depositing the Ni film.

The last step was the lift-off process, which was processed in an AZ-Kwik Strip Remover (AZ Electronic Materials). In this process, the Ni patterns with photoresist underneath were washed away, while the Ni patterns without photoresist underneath stayed. Thus, the Ni patterns obtained were the same as that in the mask.

Platinum (Pt) cathodes and Pt reference electrodes with thickness of 100 nm were deposited by DC magnetron sputtering. The Pt cathode (not patterned) was placed symmetrically to the pattern

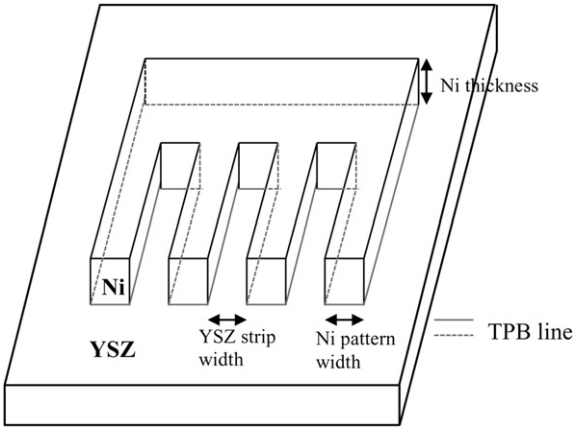

Fig. 2. Schematic geometry of the SOFC with Ni/YSZ pattern anode.

Table 1
DC magnetron sputtering parameters for Ni film deposition.

Parameters	Value (unit)
Sputtering gas flow rate	30 sccm
Basis pressure in the chamber	6.7×10^{-6} mbar
Pressure during sputtering	5.1×10^{-3} mbar
Power provided at the target	400 W
Sputtering rate	1 μm h^{-1}

anode on the opposite side of the YSZ single crystal. Configurations of the Ni/YSZ pattern anode, Pt cathode and Pt reference electrode are given in Fig. 3.

2.2. Characterization of Ni/YSZ pattern anodes

A microscope equipped with a high-resolution digital camera and an imaging system was used to generate images from the samples.

LEO 1530 SEM and energy-dispersive X-ray spectroscopy (EDX) were used in this study to characterize the Ni/YSZ pattern anode microstructure and composition. Due to the low conductivity of the Ni/YSZ pattern anode, a thin gold film was deposited on the sample surface to reduce the electronic charging effects.

The thickness of Ni pattern was measured by a Sloan (Veeco) Dektak-I Profilometer System, which is a contact profilometer system equipped with PC interface. InstaCal data capture interface card and TracerDAQ data capture interface software were used to capture the substrate surface profile.

Experiments regarding the effects of Ni thickness, temperature and H_2O concentration on Ni/YSZ pattern anode structure were performed by installing the pattern anode cell in an electrochemical test system. In this system, the cell sits on co-axial alumina tubes with anode side facing down. The outer tube is used to support the cell, and it has a similar size as the cell. The inner alumina tube works as a fuel pathway to supply the desired fuel to the anode. During the experiments, the fuel flows toward the anode side through the inner alumina tube and leaves through the annulus space between the outer and inner alumina tubes to the exhaust outlet.

LabVIEW–field point program is used in this test system to control H_2 and N_2 gas composition changes. In this setup, humidified fuels with any desired water content can be achieved through a water bubbler system (3% H_2O) or a Controlled Evaporation and Mixing system (CEM, Bronkhorst).

A Solartron Frequency Response Analyzer 1260 and a Solartron Electrochemical Interface 1287 were used for electrochemical impedance spectroscopy (EIS) measurements. The frequency range used in the measurement was from 0.1 Hz to 10^5 Hz. An excitation voltage of 10 mV was used to ensure that the measurement was performed in the linear regime. Three electrodes configuration was applied to characterize the Ni/YSZ pattern anode electrochemical behavior. Polarization resistance (R_p) is the difference of the low frequency intercept and the high frequency intercept on the real-axial of the Nyquist plot.

3. Results and discussion

3.1. Optimization of Ni/YSZ pattern anode fabrication conditions

PGMI SF11 was used as the sacrificial layer. Resists ma-N-1420 and nLOF2035 were chosen as imaging layers. The spin and soft-bake conditions for PGMI SF11 were the same when these two imaging photoresists were used as the top layer separately. For both ma-N-1420 and nLOF2035, the spin speed and soft-bake conditions were referred to manufacture recommended conditions, although optimization around the recommended conditions was also performed. The exposure time and development time were also optimized. It was found that the development time was the most critical parameter for the successful fabrication of Ni patterns. If the soft-bake temperature is fixed, the development time directly affects the size of undercut, which should not be too small or too big. If the undercut is too small, the side wall of Ni film will connect with the horizontal film after sputtering, which makes the lift-off impossible. If the undercut is too big, the resist pattern structure will be destroyed. So it is very important to get a suitable size of undercut. However, the undercut size is very hard to measure. Besides, the undercut size changes from batch to batch. A significant number of experiments revealed that the development time of 1–2 min recommended by the manufacture is far from enough for a suitable undercut formation. It was determined that a development time around 8 min was best. In one experiment, the development time was extended to 9 min, at which point the resist started to peel off. This means that the undercut was too

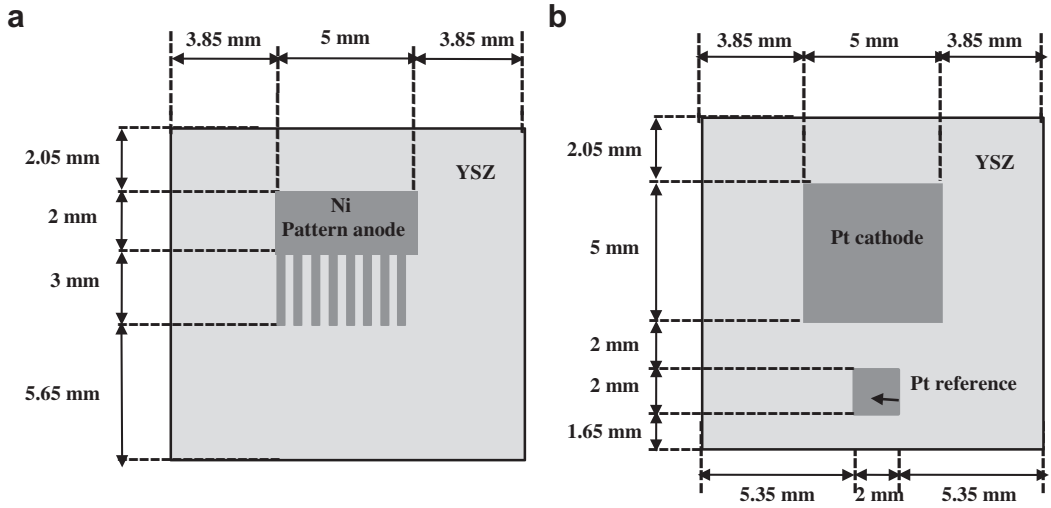

Fig. 3. Schematic top view design of Ni/YSZ pattern anode, Pt cathode and Pt reference electrode. Ni and YSZ strips have the same width. The Pt cathode (not patterned) was placed symmetrically to the pattern anode on the opposite side of the YSZ.

big. In the following experiments, the development time was controlled between 8 and 8.5 min. It turned out that precise patterns were made after lift-off using this method. The light microscope photographs of the nLOF2035 resist structure with different development times are shown in Fig. 4(a) and Fig. 4(b).

Fig. 4(a) presents the resist patterns after developing for 8 min. The development time for the resist patterns shown in Fig. 4(b) is according to the manufacture's recommendations (1.5 min). Fig. 4(a) shows semi-circle wrinkles on the resist side, which is caused by the overdevelopment of the resist. The semi-circle wrinkles also indicate that big undercuts are formed. If the development time is not long enough, these semi-circle wrinkles will not appear, just as what is shown in Fig. 4(b). This is a very simple, fast and effective way to identify if the undercut size is adequate.

After making the resist patterns, Ni was deposited by DC magnetron sputtering. Fig. 5 gives the overview of the pattern after Ni deposition, which shows clean and smooth Ni film layer.

Three different types of Ni pattern anodes were prepared. The Ni pattern widths were 100 μm, 50 μm and 20 μm. These three types of patterns are shown in Fig. 6. On the one hand, the Ni pattern edges for these three Ni/YSZ pattern anodes are sharp and precise. On the other hand, the patterns are not exactly the same as those of the mask. For the mask, the Ni strip width and the YSZ strip width are the same, whereas the Ni strip width is wider than the YSZ strip width in the final product. This was due to the overdevelopment of the resist. The difference between the Ni and YSZ strip width increases with decreasing the pattern width from 100 μm to 20 μm. Thus, the real Ni area is bigger and the TPB length is shorter compared to the theoretical value. However, the real TPB length can still be easily and accurately calculated.

EDX analysis showed that the Ni surface was composed of pure Ni, and no oxide Ni or other contaminated elements existed.

The photolithographic conditions for photoresist ma-N-1420 were also optimized in a similar way as what was done for nLOF2035. However, Ni patterns could not be successfully made. In the lift-off step, although the recommended organic solvent mixture remover PG was used, the unwanted Ni could not be nicely removed. Although the big feature (2 × 2 mm) could be obtained, small Ni patterns peeled off from the YSZ. Thus, it was very hard to control the Ni pattern quality using ma-N-1420. Therefore, nLOF2035 was chosen as the imaging resist in Ni pattern anodes fabrication.

3.2. Ni/YSZ pattern anode microstructure changes in H_2–H_2O atmosphere

Three types of Ni pattern anodes with Ni thickness of 0.5 μm, 0.8 μm and 1 μm were fabricated. Ni pattern microstructure changes with Ni thickness, temperature and H_2O concentration were characterized.

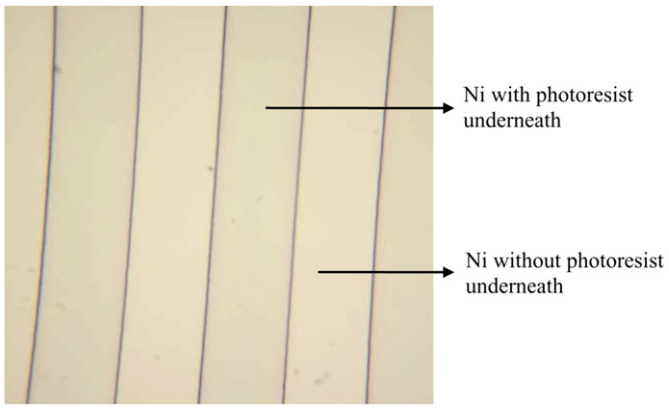

Fig. 5. Patterns after Ni deposition by DC sputtering.

In Fig. 7, a group of Ni/YSZ pattern anodes with Ni thickness of 0.5 μm are presented in SEM photographs. SEM photograph of Ni patterns just after fabrication is shown in Fig. 7(a). Sharp and precise TPB were obtained after the pattern anode fabrication. Besides, the Ni grain size is very small and distributed evenly. Fig. 7(b) presents heat treatment effects in N_2 on Ni/YSZ pattern anodes at 550 °C for 20 h. In this case, the TPB still remains sharp and straight. However, the Ni grain size increased compared to the Ni pattern before the heat treatment. In Fig. 7(c), the Ni/YSZ pattern anode sample was exposed to N_2 and H_2 mixtures at 550 °C for 20 h. The pattern on the top image of Fig. 7(c) is very similar to that on the top image of Fig. 7(b), indicating that the presence of dry H_2 has only a small effect on the TPB line. However, comparison between the bottoms images of Fig. 7(b) and (c) shows that the Ni particles started to aggregate after the experiments where the patterned anode was exposed to dry H_2. The Ni/YSZ pattern anode sample shown in Fig. 7(d) was treated in N_2 and humidified H_2 with 3% water at 700 °C for 12 h. After the test, part of the Ni patterns delaminated from the YSZ and holes were also formed on the remaining Ni patterns, which showed a network structure. The high magnification SEM images exhibited the aggregation of Ni particles.

Another series of Ni/YSZ pattern anode samples with Ni thickness of 0.8 μm was evaluated in a similar way and the results are shown in Fig. 8. Fig. 8(a) shows that heat treatment at 550 °C in N_2 for 20 h on the sample did not impact the TPB line. When the sample was exposed to N_2/H_2 gas mixtures with H_2O mole fractions

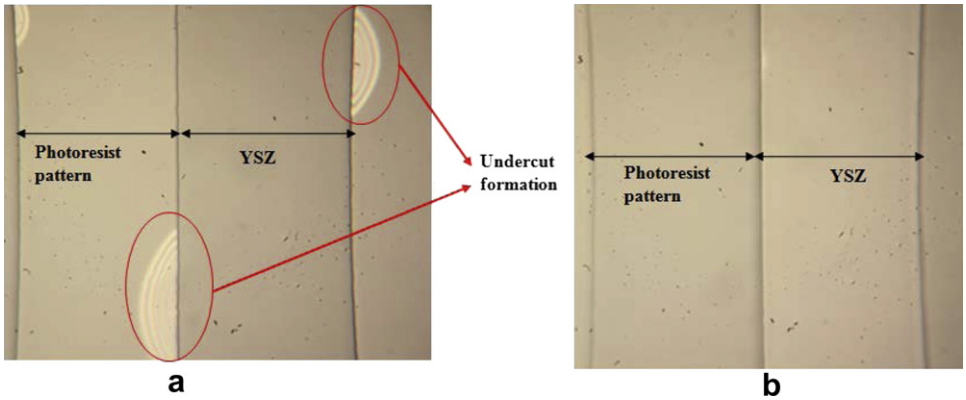

Fig. 4. Patterns of photoresist after development (a) long development time with big undercut formation, (b) short development time without sign of big undercut formation.

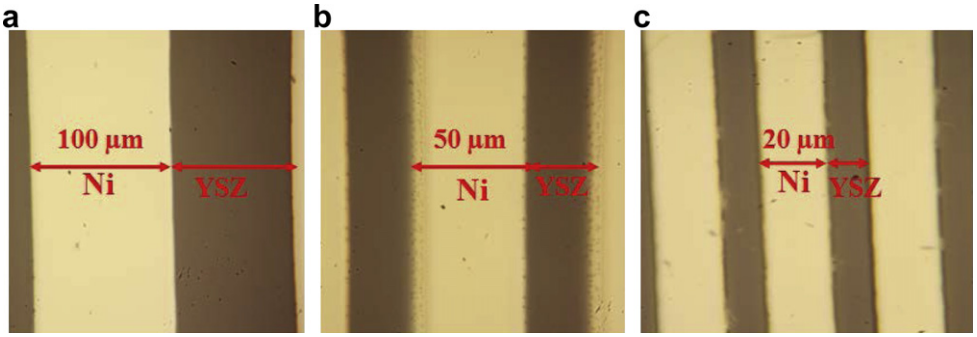

Fig. 6. Ni patterns with different Ni strip width (a) 100 μm, (b) 50 μm, (c) 20 μm.

in the range 3–50% at 550 °C for 20 h, the TPB line also did not change, as seen in Fig. 8(b). However, the Ni particles became much larger. In Fig. 8(c), the sample was tested under the same conditions as the sample in Fig. 8(b) except that the temperature was increased to 700 °C. After the electrochemical test, none of the Ni patterns peeled off, but holes were formed on the Ni patterns, and network structure appeared. Therefore, the TPB length experienced dramatic changes. In Fig. 8(d), Ni/YSZ pattern anode sample with the same thickness (0.8 μm) was tested with humidified H_2 (3% H_2O) at 700 °C, the TPB line did not show significant change. Results from Fig. 8(b)–(d) highlight the deleterious effect of water on the Ni pattern microstructure at higher temperatures (e.g. 700 °C).

In another experiment, the SOFC with 0.8 μm thick Ni pattern anode was heated up to 800 °C with 3% H_2O added to the H_2 fuel. After the electrochemical test, most parts of the Ni pattern maintained dense structure, but some holes appeared. Besides, the Ni pattern edges were not as smooth and sharp any more. The SEM image in Fig. 9(a) describes the Ni pattern changes. More holes in the Ni pattern were observed when the H_2O content was increased to 10%, which is shown in Fig. 9 (b).

Ni/YSZ pattern anodes with 1.0 μm thick Ni were also tested in H_2 environments with different H_2O content.

Fig. 10 shows the Ni pattern after being tested in H_2 with 3% H_2O in the temperature range of 500–800 °C. There were no holes formed under this condition, but the Ni pattern edge was modified, which leads to an increase in TPB length. This would not be as much of a problem as through imaging techniques it is possible to calculate the new TPB length.

However, the presence of higher amount of H_2O (3–70%) at 700 °C considerably altered the Ni pattern microstructure as seen in Fig. 11 where the Ni pattern was characterized with SEM after the test. Holes formed in the Ni pattern, and Ni was found to be in the oxidized state (confirmed by EDX). For such microstructure it becomes impossible to determine (or even estimate) the actual TPB length.

Sukeshini et al. [12] employed Ni/YSZ pattern anodes to investigate the electrochemical oxidation of H_2, CO and H_2/CO mixtures. The Ni thickness in their study was 0.1–0.15 μm, and all the patterns turned into island structure after electrochemical tests at 735–850 °C in both dry H_2 and wet H_2 (4% H_2O) environments. Utz et al. [9] evaluated the microstructure changes of Ni/YSZ pattern anode under different conditions of temperatures and partial pressures of H_2 and H_2O. Partly interconnected islands formed on the thin Ni layers (0.15 μm and 0.2 μm), whereas holes formed on the thicker Ni layers (0.4 μm) after experiments where the temperature ranged from 550 to 800 °C in dry H_2 environment. Ehn et al. [11] also observed Ni islands formation for thin Ni layer (0.25 μm) in H_2 with 3% H_2O after experiments where the temperature ranged from 350 to 500 °C. Holes formation was also observed when using thicker Ni layer (0.25–0.5 μm) in humidified H_2 (3% H_2O) after experiments where the temperature ranged from 400 to 700 °C. Ni pattern with Ni thickness of 1.0 μm kept its

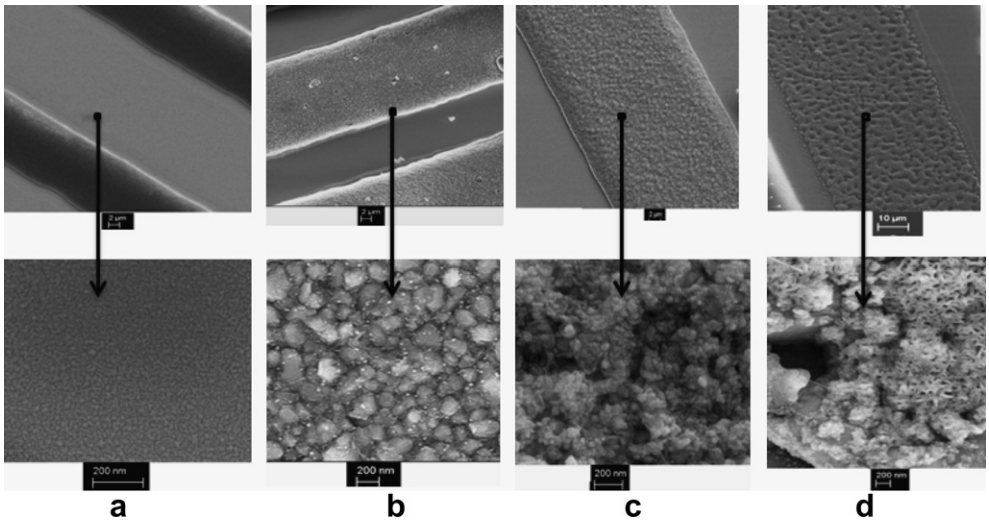

Fig. 7. The effects of temperature, H_2, and H_2O on 0.5 μm thick Ni patterns (a) Ni patterns after fabrication, (b) Ni patterns after heat treatment in N_2at 550 °C for 20 h, (c) Ni patterns after exposure to N_2 and dry H_2 (20%) mixture for 20 h at 550 °C, (d) Ni patterns after exposure to N_2 and humidified H_2 (20%) with 3% H_2O at 700 °C for 12 h.

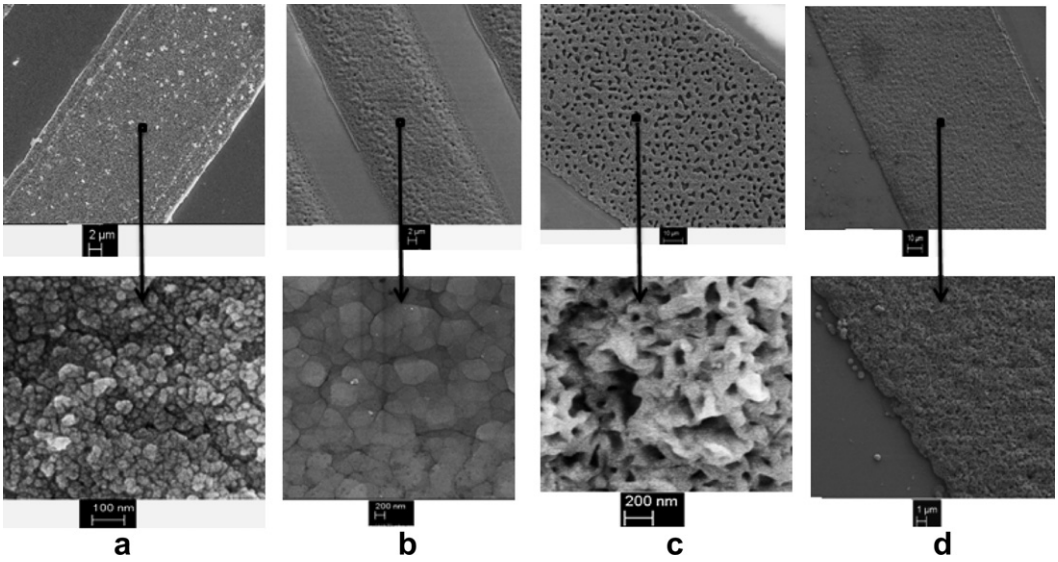

Fig. 8. The effects of temperature, H_2, and H_2O on 0.8 μm thick Ni patterns (a) Ni patterns after heat treatment in N_2at 550 °C for 20 h, (b) Ni patterns after exposure to N_2 and H_2 mixture (20%) with 3–50% H_2O for 20 h at 550 °C, (c) Ni patterns after exposure to N_2 and H_2 (20%) with 3–50% H_2O at 700 °C for 24 h, (d) Ni patterns after exposure to the mixture of N_2 and H_2 (50%) with 3% H_2O at 700 °C for 24 h.

original shape with the Ni pattern edge slightly modified in humidified H_2 (3% H_2O) at 700 °C. In our study, 0.5 thick Ni patterns showed stable structure only in dry H_2 environments at 550 °C or below. When the temperature was increased to 700 °C, holes appeared on the Ni pattern. Ni pattern with Ni thickness of 0.8 μm remained a dense structure when the cell was tested in both dry H_2 and humidified H_2 (3–70% H_2O) at 550 °C. At 700 °C and 800 °C, holes formed when the H_2O content was between 5 and 70%. Holes formation happened when using 1.0 μm thick Ni at 700 °C for H_2O content of 10% and above. Our observations regarding the stability of the patterned anode in the presence of water was thus different from those of Utz et al. [9] who suggested that the Ni pattern anode microstructure was maintained stable during electrochemical with high amount of H_2O (>20%) in the temperature range of 700–900 °C when the Ni thickness was 0.8 um or above.

3.3. Ni/YSZ pattern anode electrochemical behavior in H_2–H_2O atmosphere

The electrochemical behavior of the Ni/YSZ pattern anode with 1.0 μm thick Ni was characterized by EIS in H_2 environments with H_2O content from 3 to 70% in the temperature range of 550–800 °C. Fig. 12(a) gives EIS Nyquist plots of experimental and equivalent circuit fitting results for a fuel composed of 50% H_2 and 3% H_2O at 700 °C. Fig. 12(b) presents the equivalent circuit model used for the fitting. In this equilibrium circuit model, Rs(R1CPE1)(R2CPE2), Rs represents pure ohmic resistance, R1 and R2 are resistances related to activation polarization, and CPE1 and CPE2 are constant phase elements. There are two main semi-circles in the impedance Nyquist plot. The polarization resistance for the first and second semi-circles (R1 and R2) are 112.5 $\Omega \cdot cm^2$and 21.3 $\Omega\ cm^2$, respectively.

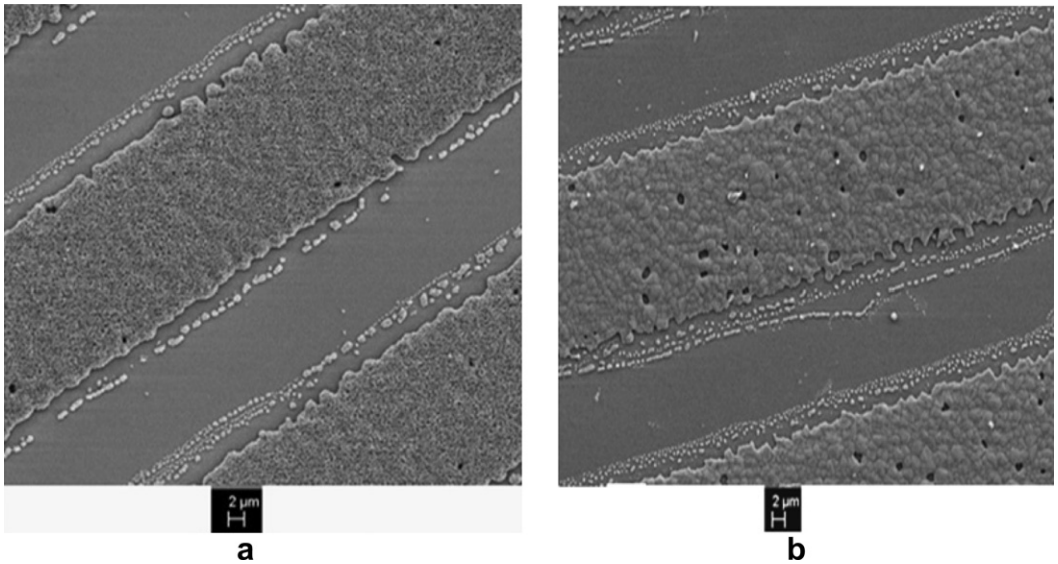

Fig. 9. SEM images of 0.8 μm thick Ni patterns after electrochemical tests in different conditions (a) gas composition: N_2, H_2 (50%), H_2O (3%); T: 500–800 °C; test time: 46 h, (b) gas composition: N_2, H_2 (50%), H_2O (3–10%); T: 500–800 °C; test time: 46 h.

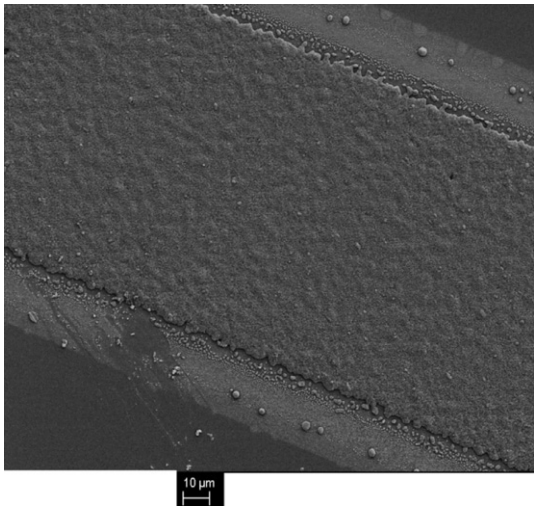

Fig. 10. SEM images of the Ni pattern with 1.0 μm thickness after being tested in H_2 (50%) with 3% H_2O in the temperature range of 500 °C–800 °C.

In previous studies, one main semi-circle was mentioned for impedance spectra in H_2 environments by Mizusaki et al. [8] and Bieberle et al. [5]. In de Boer's study [3] three semi-circles were obtained through equivalent circuit fitting for H_2 electrochemical tests. In H_2 environment, Ehn et al. [11] observed two main semi-circles in the impedance spectra whereas Sukeshini et al. [12] observed one conductive circle and one resistance circle. In Utz et al.'s study [7] electrochemical impedance test revealed three semi-circles, which were attributed to gas diffusion, charge transfer process in the pattern anode and a process caused by the counter electrode. Our pattern fabrication method is similar to that in the work of Utz et al. The fact they observed three semi-circles, whereas we observed two could be attributed to the two-electrode system they used vs. the three-electrode configuration in our study.

In the following experiment, polarization resistance changes with time at different temperatures with 3% H_2O and 10% H_2O were monitored, and they are shown in Fig. 13(a) and Fig. 13(b). Meanwhile, Table 2 gives the initial polarization resistances as well as the degradation rates after each change in the temperature. The cell was first tested in H_2 with 3% H_2O at 700 °C for 7 h, when the polarization resistance increased at a rate of 5.3 Ω cm^2 h^{-1} during this period. The temperature was then increased to 750 °C for 2 h, during which the polarization resistance degradation rate reached 6.4 Ω cm^2 h^{-1}. When the temperature was lowered to 700 °C again, the polarization resistance degradation rate (2.8 Ω cm^2 h^{-1}) was lower than that of the first 7 h. This means that the Ni pattern microstructure stabilizes faster at 750 °C compared to 700 °C.

The temperature was increased from 700 to 800 °C, after which the polarization resistance degradation rate was 5.0 Ω cm^2 h^{-1} over a 2 h period. The experiment continued by decreasing the temperature to 750 °C, which yielded a polarization resistance degradation rate of 2.3 Ω cm^2 h^{-1}. The degradation rate of polarization resistance (2.3 Ω cm^2 h^{-1}) at 750 °C is lower than the 6.4 Ω cm^2 h^{-1} tested at 750 °C before increasing the temperature to 800 °C, which can be related to faster Ni microstructure stabilization at higher temperature.

The increase in polarization resistance with time is attributed to the shortening of the TPB length. Two modes for shortening the TPB length could be proposed: 1) shortening of the TPB length at the edge of the pattern and 2) shortening of the TPB length due to nanopores being filled. In both modes, when the cell is heated, the Ni grain size becomes bigger (e.g. see Fig. 7(b) and Fig. 8(b), and the Ni particles start to migrate due to the thermal stress. The growth in Ni grain size smoothens the pattern edge, which in turn can contribute to the shortening of TPB length [19].

At the same time, nanopores in the Ni pattern, which also contribute to the TPB length, are filled with the migrated Ni particles. Thus, the TPB length becomes shorter with more nanopores being filled with the migrated Ni particles [8].

When the temperature was lowered to 550 °C, and then increased to 700 °C, the polarization resistance was very similar to the value before the cell experienced lowering the temperature. This indicates that when the temperature is below 700 °C, temperature does not have any effect on the Ni pattern microstructure.

When the H_2O content was increased to 10%, the degradation rate of polarization resistance was 17.3 Ω cm^2 h^{-1} at 700 °C, which was higher than that with 3% H_2O (6.9 Ω cm^2 h^{-1}). When the cell was heated to 750 °C with 10% H_2O, a degradation rate of 11.9 Ω cm^2 h^{-1} was obtained. The temperature was then lowered to 700 °C, and the degradation rate became 6.2 Ω cm^2 h^{-1}. The lower

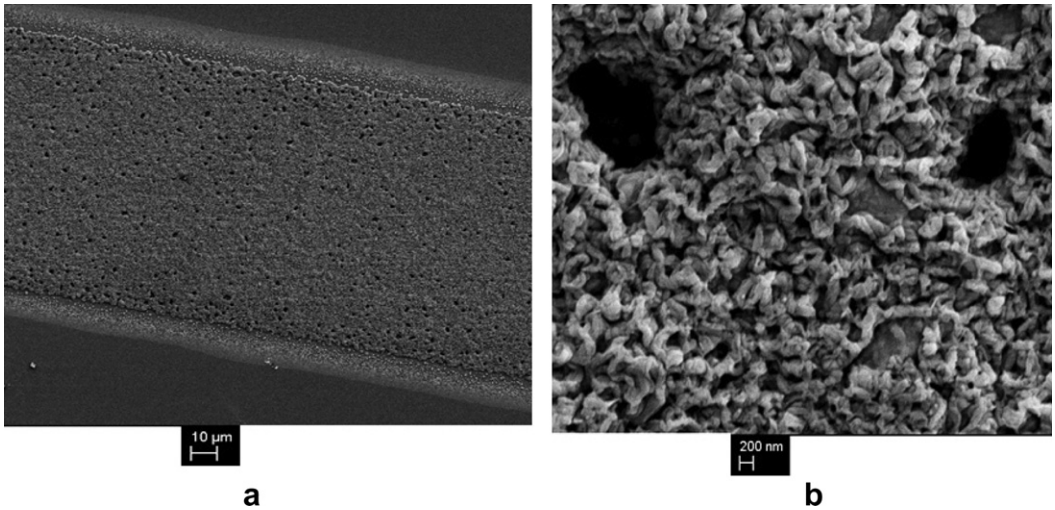

Fig. 11. Schematic view of microstructural changes in the Ni pattern after electrochemical test in H_2 (20%) with H_2O content in the range of 3–70% (a) low magnification, (b) High magnification.

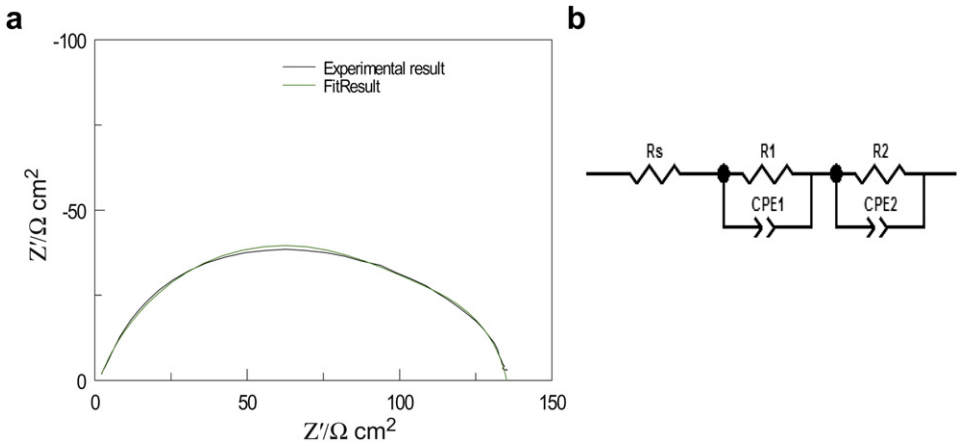

Fig. 12. (a) Experimental and fitting impedance plots when the test was performed in 50% H_2 with 3% H_2O at 700 °C, (b) Equilibrium circuit fitting model.

degradation rate indicates that the TPB length may have increased, likely due to holes formation in the Ni pattern. The polarization resistance degradation rate at 800 °C was 3.9 Ω cm^2 h^{-1}, which later became 5.5 Ω cm^2 h^{-1} when the temperature was lowered to 750 °C. The polarization degradation rate at 750 °C of 5.5 Ω cm^2 h^{-1} is much lower than that obtained at the same temperature, but 4 h before (11.9 Ω cm^2 h^{-1}). Again, this may due to the increase of TPB length. After that the temperature was changed back to 700 °C the degradation rate became 20.6 Ω cm^2 h^{-1}. The increased degradation rate after 40 h test was due to delamination of Ni layer, which was observed after the electrochemical test. When the temperature was lowered to 650 °C, the polarization resistance reached 615.7 Ω cm^2, and the degradation rate became 64.4 Ω cm^2 h^{-1}. These values are much higher than the values in Fig. 13(a) when the H_2O content is 3% at the same temperature. The polarization resistance increased to 2500 Ω cm^2 with further decreasing the temperature to 600 °C, and the corresponding degradation rate was 87.3 Ω cm^2 h^{-1}.

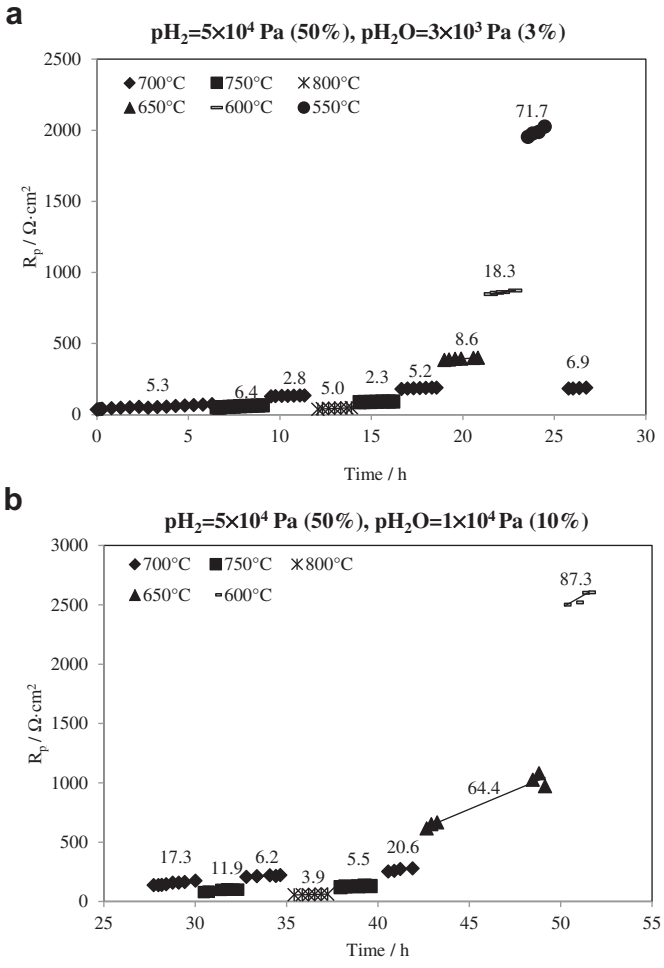

Fig. 13. Polarization resistance changes of 1.0 μm thick Ni/YSZ pattern anode with time at different temperatures in 50% H_2 (a) 3% H_2O, (b) 10% H_2O.

In previous studies, de Boer [3], Mizusaki et al. [8] and Ehn et al. [11] observed an increase in polarization resistance with time when the Ni/YSZ pattern anodes were tested in H_2 environment. In our study, we observed the same trend. However, Utz et al. [7,9] claimed that the polarization resistance decreased with time in the first 25 h, and then, a stable cell performance was achieved when the Ni thickness was 0.8 or above. Since our anode pattern fabrication method was closest to that of Utz et al. it is surprising that the results are so different, but we have no explanation at the present time.

In order to further evaluate the effects of H_2O on Ni/YSZ pattern anode electrochemical behavior, another experiment was carried out to characterize the polarization resistance changes with time with H_2O content varying from 3 to 70%. Results are shown in Fig. 14 and Table 3. Similar to the experiment related to Fig. 13, the cell was first tested in H_2 environment with 3% H_2O at 700 °C. The degradation rate was measured at 37.3 Ω cm^2 h^{-1} under these conditions. The H_2O content was then increased to 10% for 1 h and

Table 2
Initial polarization resistances and degradation rates after each variation in temperature.

Temperature (°C)	3% H_2O		10% H_2O	
	Initial R_p (Ω cm^2)	Degradation rate (Ω cm^2 h^{-1})	Initial R_p (Ω cm^2)	Degradation rate (Ω cm^2 h^{-1})
700	32.5	5.3	137.6	17.3
750	49.8	6.4	78.8	11.9
700	128.0	2.8	207.3	6.2
800	37.0	5.0	55.1	3.9
750	87.3	2.3	120.6	5.5
700	179.0	5.2	251.7	20.6
650	383.0	8.6	615.7	64.4
600	820.6	18.3	2500.0	87.3
550	1952.8	71.7	–	–
700	181.9	6.9	–	–

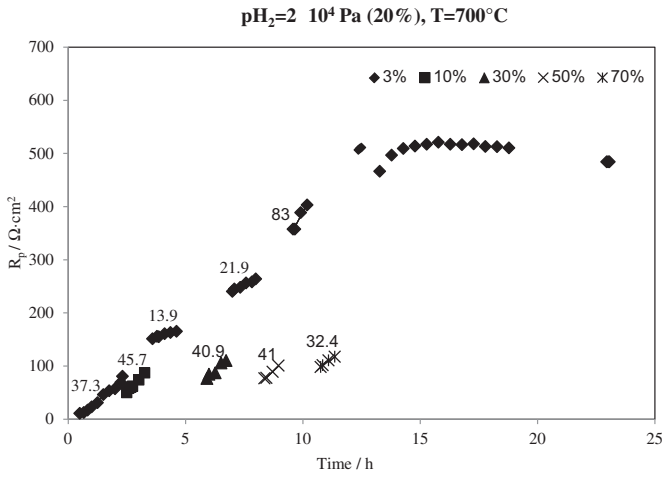

Fig. 14. Polarization resistance changes with time in H_2 (20%) with H_2O content from 3 to 70% at 700 °C.

was then decreased to 3%. The polarization resistance degradation rates were 45.7 Ω cm^2 h^{-1} at 10% H_2O and 13.9 Ω cm^2 h^{-1} at 3% H_2O. Subsequently, the H_2O content was increased to 30% from 3%, and then decreased back to 3%. The polarization resistance rate changed from 40.9 Ω cm^2 h^{-1} at 30% H_2O to 21.9 Ω cm^2 h^{-1} at 3% H_2O. This value was still lower than the initial degradation rate (37.3 Ω cm^2 h^{-1}). The cell was then exposed to 50% H_2O for 1 h with a degradation rate of 41 Ω cm^2 h^{-1}. Then the H_2O concentration was decreased back to 3%, and the polarization resistance degradation rate became 83 Ω cm^2 h^{-1}, which is much higher than the 37.3 Ω cm^2 h^{-1} observed previously. This means that cell exposure to 50% H_2O at 700 °C severely degraded the polarization resistance. After that the cell was exposed to 70% H_2O for 1 h and then back to 3% H_2O, at which point the polarization resistance started to stabilize around 500 Ω cm^2. The polarization resistance degradation rate was 32.4 Ω cm^2 h^{-1} when the H_2O content was 70%. Another experiment at 700 °C (not shown here) where the H_2O content was kept constant at 3% for 25 h showed that the polarization resistance increased linearly without reaching a plateau. This demonstrated that the presence of higher amount of water helped in stabilizing the polarization resistance.

The inconsistent results regarding Ni/YSZ electrochemical behavior in H_2–H_2O environments from literature, which was mentioned in Section 1.3, could be due to the inaccurate estimation of real TPB length and eventually to different times at which data were collected. All electrochemical tests should be performed only after a stable Ni pattern microstructure is achieved. SEM characterization should be done after each test in order to accurately calculate the TPB length. This becomes especially important when the cell is exposed to various amounts of water, for example when performing experiments to validate H_2 electro–chemical reactions mechanism.

Table 3
Initial polarization resistances and degradation rates after each variation in water content.

H_2O content (%)	Initial R_p (Ω cm^2)	Degradation rate (Ω cm^2 h^{-1})
3	10.6	37.3
10	49.5	45.7
3	151.0	13.9
30	76.2	40.9
3	240.0	21.9
50	76.7	41.0
3	375.1	83.0
70	98.0	32.4
3	506.2	–

4. Conclusion

Photolithographic process with a bi-layer resist system is an effective way for well-defined Ni/YSZ pattern anode fabrication. In this study, imaging resist nLOF2035 and sacrificial resist PGMI SF11 were found to be effective in the bi-layer photolithographic process. A simple way, involving microscopic photograph of photoresist pattern, to check if the undercut size is big enough for the lift-off was proposed; semi-circle wrinkles shown in the photograph indicates that the undercut is big enough for successful pattern anode fabrication.

A comprehensive set of experiments were conducted with H_2–H_2O mixtures to evaluate the effects of Ni thickness (0.5–1 μm), temperature (500–800 °C), and H_2O concentrations (3–70%) on Ni/YSZ pattern anode microstructure and electrochemical behavior changes.

Ni/YSZ pattern anodes with Ni thickness of 0.5 μm led to significant changes in the TPB length above 550 °C and are, therefore, not suitable for electrochemical tests. Only experiments with dry H_2 at 550 °C led to stable patterns.

Ni/YSZ pattern anodes with Ni thickness of 0.8 μm was suitable for all dry H_2 and humidified H_2 (3–50% H_2O) tests at 550 °C, as no significant changes in TPB line were observed. At 700 °C, the TPB line does not change for tests carried out with dry and humidified (3%) H_2. More holes formed when the water content was increased to 10% or above. At 800 °C, the TPB line experienced coarsening and some holes appeared in the Ni pattern when the cell was exposed to 3% H_2O.

Ni/YSZ pattern anodes with Ni thickness of 1.0 μm maintained its dense structure when the cell was tested in H_2 with 3% H_2O in the temperature range of 500–800 °C. However, the TPB length still experienced dramatic change when the test was conducted in H_2 with 10–70% H_2O at 700 °C. The significant effects of high H_2O content (>3%) on the TPB length at high temperature (e.g. 700 °C) requires the tests involving high H_2O content to be conducted at relatively lower temperature (e.g. 550 °C).

Stability tests about impedance measurements were carried out for the 1.0 μm thick Ni pattern in H_2 with 3% H_2O. The time to reach stable impedance measurements is correlated to the temperature: the Ni pattern microstructure stabilized faster when the temperature was increased to 750 °C or 800 °C (where it took ∼20 h) compared to 700 °C (where it took more than 50 h). Thus, before performing any electrochemical tests, the cell could be pre-treated under humidified H_2 at 750 °C or 800 °C until achieving a stable microstructure.

Acknowledgments

This research was supported through funding to the NSERC Solid Oxide Fuel Cell Canada Strategic Research Network from Natural Science and Engineering Research Council (NSERC) and other sponsors listed at www.sofccanada.ca. The authors gratefully acknowledge the group of Center for Integrated RF Engineering (CIRFE) at the University of Waterloo for allowing us to use their clean room facilities and their technical support during the Ni/YSZ pattern anodes fabrication.

References

[1] N.Q. Minh, T. Takahashi, Science and Technology of Ceramic Fuel Cells, first ed., Elsevier Science, 1995, p. 378.

[2] R. O'Hayre, S. Cha, W. Colella, F.B. Prinz, Fuel Cell Fundamentals, John Wiley & Sons, Hoboken, N.J., 2006, p. 409.
[3] B. Boer de, PhD Thesis, University of Twente, Twente, 1998.
[4] A. Bieberle, L.J. Gauckler, Solid State Ionics 135 (2000) 337–345.
[5] A. Bieberle, L.P. Meier, L.J. Gauckler, J. Electrochem. Soc. 148 (2001) A646–A656.
[6] M. Vogler, A. Bieberle-Hütter, L. Gauckler, J. Warnatz, W.G. Bessler, J. Electrochem. Soc. 156 (2009) B663–B672.
[7] A. Utz, H. Störmer, A. Leonide, A. Weber, E. Ivers-Tiffée, J. Electrochem. Soc. 157 (2010) B920.
[8] J. Mizusaki, H. Tagawa, T. Saito, J. Electrochem. Soc. 141 (1994) 2129–2134.
[9] A. Utz, H. Störmer, D. Gerthsen, A. Weber, E. Ivers-Tiffee, Solid State Ionics 192 (2011) 565–570.
[10] A. Utz, A. Leonide, A. Weber, E. Ivers-Tiffée, J. Power Sources 196 (2011) 7217–7224.
[11] A. Ehn, J. Høgh, M. Graczyk, K. Norrman, L. Montelius, M. Linne, M. Mogensen, J. Electrochem. Soc. 157 (2010) B1588.
[12] A.M. Sukeshini, B. Habibzadeh, B.P. Becker, C.A. Stoltz, B.W. Eichhorn, G.S. Jackson, J. Electrochem. Soc. 153 (2006) A705.
[13] T.M. Adams, R.A. Layton, Introductory MEMS Fabrication and Applications, Springer, New York, USA, 2010, pp.446.
[14] E. Koep, Ph.D Thesis, Georgia Institute of Technology, Atlanta 2006.
[15] O. Cherry, Master Thesis, University of Waterloo, Waterloo, Canada, 2007.
[16] D.M. Mattox, Handbook of Physical Vapour Deposition (PVD) Processing, second ed., William Andrew Applied Science, Oxford, UK, 2010.
[17] D. Beckel, A. Bieberle-Hütter, A. Harvey, A. Infortuna, U. Muecke, M. Prestat, J. Rupp, L. Gauckler, J. Power Sources 173 (2007) 325–345.
[18] H. Geng, Semiconductor Manufacturing Handbook, The McGraw-Hill Inc, New York, 2005.
[19] R.J. Aaberg, R. Tunold, M. Mogensen, R.W. Berg, R. ødegard, J. Electrochem. Soc. 147 (1998) 2244.